proposed[21] to occur for internally excited protonated ethanol above 23 kcal/mol.[21b]

Acknowledgment. We thank the donors of the Petroleum Research Fund, administered by the American Chemical Society, and the National Science Foundation (CHE-9107121) for support for this research.

References and Notes

(1) The term distonic ion is used for radical ions which would arise (formally) by ionization of a zwitterion or a diradical. Distonic ions have charge and odd spin at separate atoms in a conventional valence bond description; α-distonic ions have charge and odd spin on adjacent atoms; β-distonic ions have one heavy atom between the charge and radical sites, and so on. See: (a) Radom, L.; Bouma, W. J.; Nobes, R. H.; Yates, B. F. *Pure Appl. Chem.* **1984**, *56*, 1831. (b) Yates, B. F.; Bouma, W. J.; Radom, L. *J. Am. Chem. Soc.* **1984**, *106*, 5805.

(2) Golding, B. T.; Radom, L. *J. Am. Chem. Soc.* **1976**, *98*, 6331.

(3) Bouma, W. J.; Nobes, R. H.; Radom, L. *J. Am. Chem. Soc.* **1983**, *105*, 1743.

(4) Terlouw, J. K.; Heerma, W.; Dijkstra, G. *Org. Mass Spectrom.* **1981**, *16*, 326.

(5) (a) Holmes, J. L.; Lossing, F. P.; Terlouw, J. K.; Burgers, P. C. *J. Am. Chem. Soc.* **1982**, *104*, 2931. (b) Burgers, P. C.; Holmes, J. L.; Terlouw, J. K.; van Baar, B. *Org. Mass Spectrom.* **1985**, *20*, 202.

(6) Wesdemiotis, C.; Danis, P. O.; Feng, R.; Tso, J.; McLafferty, F. W. *J. Am. Chem. Soc.* **1985**, *107*, 8059.

(7) Postma, R.; Ruttink, P. J. A.; Van Baar, B.; Terlouw, J. K.; Holmes, J. L.; Burgers, P. C. *Chem. Phys. Lett.* **1986**, *123*, 409.

(8) McAdoo, D. J.; Hudson, C. E. *Org. Mass Spectrom.* **1986**, *21*, 779.

(9) Ruttink, P. J. A. *J. Phys. Chem.* **1987**, *91*, 703.

(10) Ikezoe, Y.; Matsuoka, S.; Takebe, M.; Viggiano, A. *Gas-Phase Ion Molecule Reaction Rate Constants Through 1986*; Maruzen Co., Ltd.: Tokyo, Japan, 1987.

(11) (a) Chesnavich, W. J.; Su, T.; Bowers, M. T. *J. Chem. Phys.* **1980**, *72*, 2641. (b) Su, T.; Chesnavich, W. J. *J. Chem. Phys.* **1982**, *76*, 5183. (c) Bartmess, J. E.; Georgiadis, R. M. *Vacuum* **1983**, *33*, 149.

(12) Lide, D. R. *CRC Handbook of Chemistry and Physics*, 71st ed.; CRC Press: Boca Raton, FL, 1990.

(13) Lias, S. G.; Bartmess, J. E.; Liebman, J. F.; Holmes, J. L.; Levin, R. D.; Mallard, W. G. *J. Phys. Chem. Ref. Data* **1988**, *17*, Supp. 1.

(14) Wittneben, D.; Grützmacher, H.-F. *Int. J. Mass Spectrom. Ion Processes* **1990**, *100*, 545.

(15) Holmes, J. L.; Lossing, F. P. *Int. J. Mass Spectrom. Ion Processes* **1989**, *92*, 111.

(16) Busch, K. L.; Nixon, W. B.; Bursey, M. M. *J. Am. Chem. Soc.* **1978**, *100*, 1621.

(17) Hammerum, S. *Mass Spectrom. Rev.* **1988**, *7*, 123.

(18) (a) Farneth, W. E.; Brauman, J. I. *J. Am. Chem. Soc.* **1976**, *98*, 7891. (b) Olmstead, W. N.; Brauman, J. I. *J. Am. Chem. Soc.* **1977**, *99*, 4219. (c) Asubiojo, O. I.; Brauman, J. I. *J. Am. Chem. Soc.* **1979**, *101*, 3715. (d) Pellerite, M. J.; Brauman, J. I. *J. Am. Chem. Soc.* **1980**, *102*, 5993. (e) Sharma, S.; Kebarle, P. *J. Am. Chem. Soc.* **1982**, *104*, 19. (f) Caldwell, G.; Magnera, T. F.; Kebarle, P. *J. Am. Chem. Soc.* **1984**, *106*, 959. (g) McMahon, T. B.; Heinis, T.; Nicol, G.; Hovey, J. K.; Kebarle, P. *J. Am. Chem. Soc.* **1988**, *110*, 7951.

(19) See, for example: (a) Kleingeld, J. C.; Nibbering, N. M. M. *Org. Mass Spectrom.* **1982**, *17*, 136. (b) Raghavachari, K.; Chanrasekhar, J.; Burnier, R. C. *J. Am. Chem. Soc.* **1984**, *106*, 3124. (c) Sheldon, J. C.; Currie, G. J.; Bowie, J. H. *J. Chem. Soc., Perkin Trans. 2* **1986**, 941 and references therein.

(20) The relative potential energy well depths were estimated using the value 3.5 Å for the collision diameter, and following the procedure presented in the following papers: (a) Ausloos, P.; Lias, S. G. *J. Am. Chem. Soc.* **1981**, *103*, 3641. (b) Ausloos, P.; Lias, S. G. *Int. J. Mass Spectrom. Ion Processes* **1984**, *58*, 165.

(21) (a) Bouchoux, G.; Hoppilliard, Y. *J. Am. Chem. Soc.* **1990**, *112*, 9110. (b) Swanton, D. J.; Marsden, D. C. J.; Radom, L. *Org. Mass Spectrom.* **1991**, *26*, 227.

(22) Rusli, R. D.; Schwarz, H. *Chem. Ber.* **1990**, *123*, 535.

Matrix Reactions of SiH_4 and GeH_4 with F_2. Infrared Spectra of Several HF Product Complexes†

Thomas C. McInnis and Lester Andrews*

Department of Chemistry, University of Virginia, Charlottesville, Virginia 22901 *(Received: November 5, 1991; In Final Form: January 28, 1992)*

Silane and germane were condensed with F_2 at high dilution in argon on a 13 ± 1 K substrate. Weak product complexes produced on condensation and increased by ultraviolet photolysis are assigned to SiH_3F--HF, SiH_2--HF or SiH_2--$(HF)_2$, and HSiF--HF. Annealing produced new bands due to F atom reactions that are attributed to SiH_3--HF. The GeH_3F molecule was observed in the similar GeH_3F--HF complex. H-F vibrations in these complexes suggest that F is more basic in GeH_3F than in SiH_3F owing to the more electropositive nature of germanium as compared to silicon.

Introduction

Silane and germane are reactive molecules which have been studied extensively by infrared spectroscopy.[1-6] Earlier work has focused on fluorosilanes[7,8] and fluorogermanes[9,10] and the di- and trihydrides of silane and germane.[2,3,11-13] The gaseous F atom reaction with SiH_4 has been performed, and electronic spectroscopy of the SiH_3 radical has been reported.[14] However, no work has been done on the reaction of SiH_4 and GeH_4 with F atoms or F_2 in an inert matrix in order to trap several possible intermediates, although such studies have been done with CH_4 and F atoms[15] or F_2.[16] Owing to the importance of silicon and germanium in semiconductors, a better understanding of intermediates involving these elements is desired. This work was undertaken to explore the stepwise reaction of fluorine atoms and molecules with silane and germane.

Experimental Section

The vacuum and cryogenic apparatus and techniques have been described previously.[17,18] Spectra in the 4000–400-cm^{-1} region were recorded using a Nicolet 7199 FTIR spectrometer. Samples were scanned 500–1500 times at 1-cm^{-1} resolution giving a wavenumber accuracy of ±0.3 cm^{-1}. Additional spectra in the 480–200-cm^{-1} region were recorded using a Perkin-Elmer 983 infrared spectrophotometer. These matrices were scanned one to seven times at 2-cm^{-1} resolution; wavenumber accuracy is ±1 cm^{-1}.

SiH_4 (Matheson), SiD_4 (MSD Isotopes-Canada), GeH_4 (Matheson), and GeD_4 (synthesized)[5] were diluted with argon to Ar/sample ratios of 100/1, 150/1, 200/1, or 400/1. The silane or germane samples in argon were initially deposited on a CsI window at 13 ± 1 K; deposition rates, which ranged from 2 to 4 mmol/h, were controlled by varying needle valve settings. A spectrum of SiH_4, SiD_4, GeH_4, or GeD_4 in argon was recorded. Fluorine (Matheson) was diluted with argon to Ar/F_2 ratios of

---

[†] Taken in part from the M.S. Thesis of T. C. McInnis, University of Virginia, Charlottesville, VA, 1991.

0022-3654/92/2096-5276$03.00/0

TABLE I: Absorptions (cm^{-1}) of Complex 1 Formed between HF and SiH_3F and GeH_3F and Deuteriated Species in Solid Argon[a]

region	SiH_3F[b]	SiH_3F--HF	SiD_3F--DF	GeH_3F[c]	GeH_3F--HF	GeD_3F--DF
$\nu_s(HF)$		3808.9	2794.5		3676.8	2703.1
$\nu_1(SiH_3F)$	2206	2241.4	1641.2	2121		1556.8
$\nu_2(SiH_3F)$	991	978.3	707.4	859	867.4	663.2
$\nu_3(SiH_3F)$	875	793.8	784.6	689	638.1	
$\nu_4(SiH_3F)$	2209	2257.3	1647.4	2132		1572.9
$\nu_5(SiH_3F)$	961	959.9	697.2	874	881.8	668.0
$\nu_6(SiH_3F)$	729	733.4	548.6	643	667.1	477.3
		723.1	543.8			
$\nu_l(HF)$		422.4	312.6			

[a] 1 is SiH_3F--HF or GeH_3F--HF; ν_i's refer to fundamentals of the SiH_3F or GeH_3F submolecules in the complexes. [b] Reference 27. [c] Reference 29.

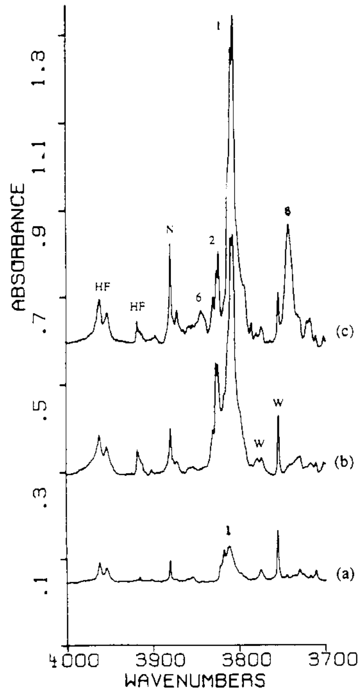

Figure 1. Infrared spectra in the 4000–3700-cm^{-1} region for $Ar/SiH_4 = 100/1$ and $Ar/F_2 = 100/1$ samples: (a) codeposited at 13 ± K, (b) after 220–1000-nm photolysis, and (c) after annealing to 25 ± 2 K.

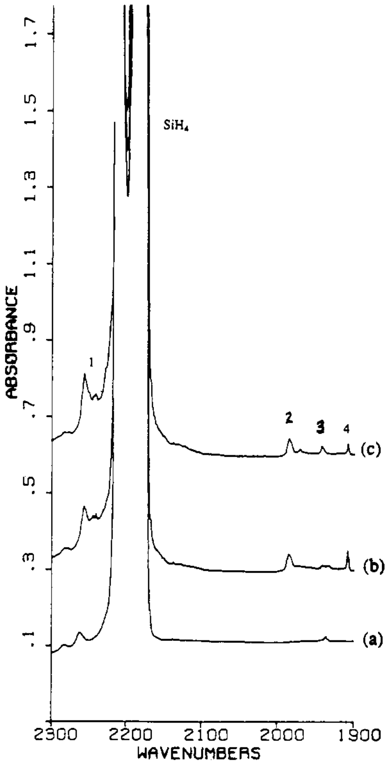

Figure 2. Infrared spectra in the 2300–1900-cm^{-1} region for sample described in Figure 1.

TABLE II: Product Absorptions (cm^{-1}) for Complexes 2 and 3 Formed between SiH_2 and GeH_2 and HF and $(HF)_2$ and Deuteriated Counterparts in Solid Argon

complex		SiH_2	SiD_2	GeH_2	GeD_2
2					
	ν_s	3828.1	2798	3730.6	2739
	ν_3	1985.7	1448.3	1870.7	1846.8
3					
	ν_3	1942.8	1424.7	1819.0	1312.5

TABLE III: Product Absorptions (cm^{-1}) of Complexes 4 and 5 Formed between HF and HSiF and HGeF and Deuteriated Species in Solid Argon[a]

complex		HSiF	DSiF	HGeF	DGeF
4					
	ν_s	3796?	2784?	3662.1	2693.2
	ν_1	1908.0	1385.4	1784.6	1287.8
	ν_2	865.5			
	ν_3	751.6			
5					
	ν_s	a		3717.2	2732.1
	ν_1	a		1795.2	1296.2

[a] Silicon counterpart was not observed.

50/1, 100/1, or 200/1, passed through a 77 K U-tube at 2–5 mmol/h, and cocondensed with the silane or germane samples for up to 9 h, and another spectrum was recorded. The sample was photolyzed with 220–1000-nm radiation from a high-pressure mercury arc (1000 W, BH6-1B, T.J. Sales, Fairfield, NJ) using a cooled 10-cm water filter for 1 h, and a spectrum was recorded. Corning glass long-wavelength pass filters were added in selected experiments. The matrix was then warmed to 23–36 K and recooled to 13 K, and another spectrum was recorded.

Results

Silane and germane samples were diluted with argon and codeposited with fluorine diluted with argon on a cold window at 13 K. New absorptions for SiH_4, SiD_4, GeH_4, and GeD_4 reactions with F_2 will be presented.

SiH_4 + F_2. Seven codeposition experiments were performed with SiH_4 and F_2 using different combinations of argon dilutions of SiH_4 (100/1 and 200/1) and F_2 (100/1 and 200/1). Infrared spectra are illustrated in Figures 1–3, and new product absorptions are listed in Tables I–III. Absorptions labeled HF at 3963.0, 3954.0, and 3919.9 cm^{-1} are due hydrogen fluoride.[19] The absorption at 3881.7, labeled N, is due to the N_2--HF complex, and the 3776.3- and 3756.3-cm^{-1} bands labeled W are due to water.[19–21] Figures 1a, 2a, and 3a show that SiH_4 and F_2 react on codeposition. In the HF stretching region, a medium-intensity band, labeled 1, was produced at 3808.9 cm^{-1}. Photolysis with a Pyrex filter, 290–1000 nm (not shown), increased the intensity of absorption 1 nearly 4-fold and produced a sharp absorption, labeled 2, at 3826.1 cm^{-1}. Full arc photolysis (Figure 1b) increased the 1 and 2 absorptions by 50%. Annealing (Figure 1c) produced a weak, broad absorption at 3846 cm^{-1}, labeled 6, and a much stronger, broad absorption at 3744 cm^{-1}, labeled 8, and the

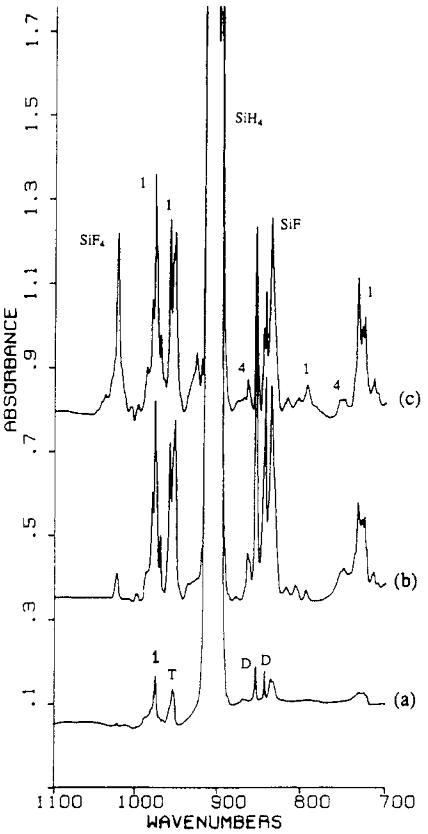

Figure 3. Infrared spectra in the 1100–700-cm^{-1} region for sample described in Figure 1.

strong 1 absorption showed further growth.

In the SiH stretching region, codeposition produced a broad band at 2257 cm^{-1} (Figure 2a). Full arc photolysis produced a new band at 2241.4 cm^{-1} labeled 1 and weak new absorptions at 1985.7, 1942.8, and 1908.0 cm^{-1}, labeled 2, 3 and 4, respectively (Figure 2b). A previous Pyrex-filtered photolysis produced approximately 75% of 2, 30% of 4, and only a trace of 3 relative to full arc photolysis. Annealing increased the yield of products 1 and 3, while 2 showed only slight growth, and 4 decreased by nearly 50% (Figure 2c).

The region near the ν_4 mode of SiH_4, which included the SiF stretching region, exhibited much action. On codeposition, a sharp band appeared at 978.3 cm^{-1} (Figure 3a). In addition, a band at 954.2 cm^{-1}, due to SiF_3 labeled T, and sharp absorptions at 855.3 and 843.7 cm^{-1} were observed due to SiF_2 labeled D. A broader absorption labeled SiF appeared at 836.8 cm^{-1}. The above bands all grew and sharpened with Pyrex photolysis, which produced 50% of the total final yield of species 1. Bands at 975.9, 959.9, 793.0, 733.4, and 723.2 cm^{-1}, labeled 1, sharpened and grew 5-fold from the weak absorptions produced upon codeposition. The T, D, and SiF bands showed marked increases as well. Full arc photolysis increased the bands labeled 1, T, D, and SiF (Figure 3b). Broad absorptions at 865.5 and 751.6 cm^{-1} increased by 300% from their initial formation in pyrex photolysis. Finally, SiF_4 appeared at 1023.3 cm^{-1}.[22]

Annealing allowed further growth of the absorptions labeled 1 (Figure 3c). The bands labeled D showed a marked decrease whereas the 4, T, and SiF bands showed slight decreases, and a new band appeared at 927.6 cm^{-1}. The SiF_4 band increased 8-fold. Spectral regions not shown revealed a strong band at 1489.1 cm^{-1} and a weaker band at 585 cm^{-1} due to O_2F on annealing[23] and thus gave further evidence of F atom diffusion and reaction. In addition a sharp band due to product 1 at 422.4 cm^{-1} formed on codeposition and increased on both photolyses and on annealing. Finally, far-IR experiments showed absorptions due to SiF_4 at 384.5 cm^{-1} and SiF_2 at 346.9 cm^{-1}.[7,22]

SiD_4 + F_2. Three codeposition experiments using SiD_4 and F_2 were performed; infrared spectra are illustrated in Figures 4–6, and new product absorptions are listed in Tables I–III.

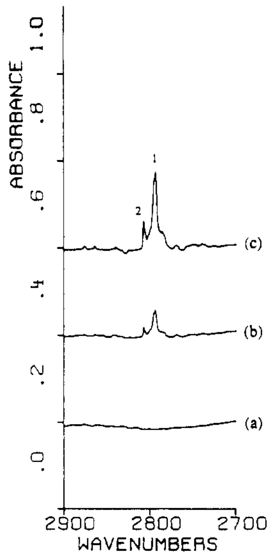

Figure 4. Infrared spectra in the 2900–2700-cm^{-1} region for Ar/SiD_4 = 100/1 and Ar/F_2 = 100/1 samples: (a) codeposited at 13 ± 1 K, (b) after 290–1000-nm photolysis, and (c) after 220–1000-nm photolysis.

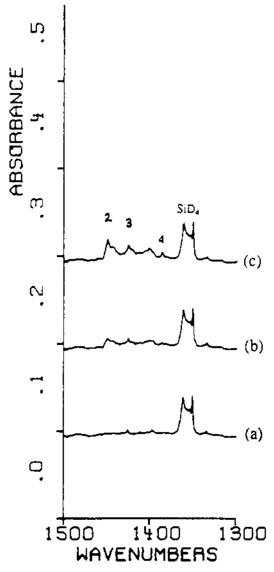

Figure 5. Infrared spectra in the 1500–1300-cm^{-1} region for sample shown in Figure 4.

Figures 4a, 5a, and 6a show that little if any reaction occurs on codeposition. In the DF stretching region, pyrex photolysis (Figure 4b) produced new absorptions at 2798.6 and 2794.5 cm^{-1}, labeled 2, and 1, respectively. Full arc photolysis (Figure 4c) produced further growth of these bands. Annealing (not shown) allowed further growth of 1 and produced a new absorption at 2755.0 cm^{-1} attributed to product 8.

The SiD stretching region revealed $2\nu_4$ of SiD_4 split at 1363.8 and 1350.9 cm^{-1}. Pyrex photolysis produced weak product absorptions at 1448.3, 1424.7, and 1385.4 cm^{-1}, labeled 2, 3, and 4, respectively, which grew further on full arc photolysis (Figure 5). The region near ν_4 of SiD_4 contained bands at 692.2 and 845.4 cm^{-1} due to $SiHD_3$[1] (Figure 6). Pyrex photolysis gave a sharp band at 836.8 cm^{-1} labeled SiF, and a new bands at 784.6, 707.4, 697.2, 548.6, and 543.8 cm^{-1}, labeled 1, and a band at 621.6 cm^{-1}, labeled 4 (Figure 6b). Full arc photolysis increase the yield of products 1, 4, and SiF (Figure 6c). The SiD_4 experiments yielded only 5–10% as much SiF_2, SiF_3, and SiF_4 as the SiH_4 experiments, which indicates that SiH_4 is much more reactive toward F_2 than SiD_4.

GeH_4 + F_2. Seven codeposition experiments were performed with GeH_4 and F_2 using different combinations of argon dilutions of GeH_4 (100/1, 150/1, 200/1, and 400/1) and F_2 (100/1 and

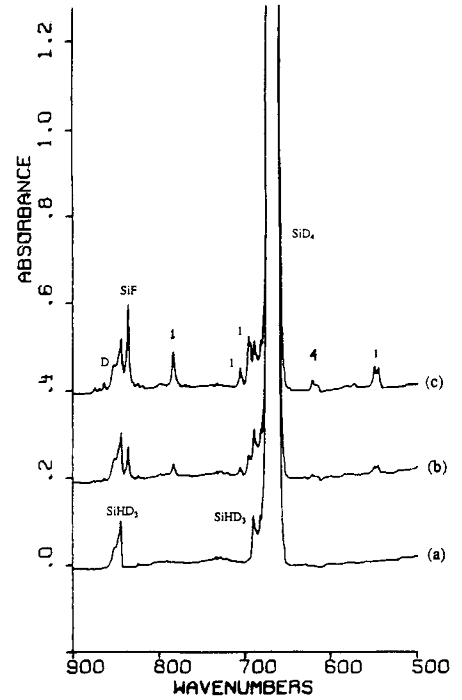

Figure 6. Infrared spectra in the 900–500-cm^{-1} region for sample shown in Figure 4.

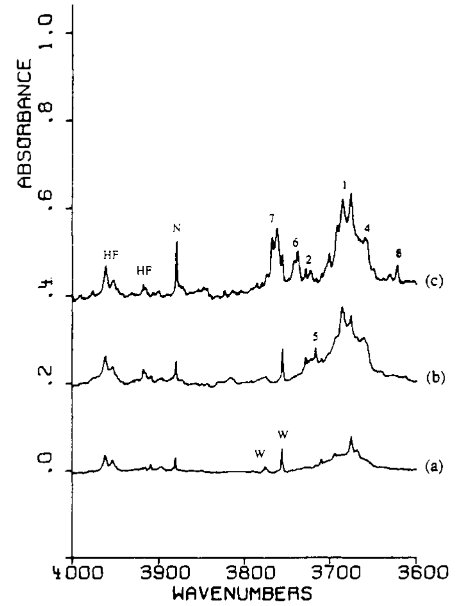

Figure 7. Infrared spectra in the 4000–3600-cm^{-1} region for Ar/GeH_4 = 400/1 and Ar/F_2 = 100/1 samples: (a) codeposited at 13 ± 1 K, (b) after 220–1000-nm photolysis, and (c) after annealing to 27 ± 2 K.

200/1). Infrared spectra are illustrated in Figures 7–9, and product absorptions are listed in Tables I–III.

GeH_4, like SiH_4, reacts on codeposition. In the HF stretching region, codeposition (Figure 7a) produced a broad absorption with a sharp peak at 3676.8 cm^{-1}, labeled 1. Pyrex photolysis (not shown) induced further growth of this band as well as producing new bands at 3717.2 and 3662.1 cm^{-1}, labeled 5 and 4, respectively. Full arc photolysis (Figure 7b) allowed for further growth of species 1, 4, and 5. Annealing (Figure 7c) produced a series of new absorptions at 3764.8, 3741.2, 3724.8, and 3624.2 cm^{-1}, labeled 7, 6, 2, and 8, respectively. The band labeled 5 decreased, while the absorptions labeled 1 increased.

In the GeH stretching region, codeposition produced two sharp bands labeled 3 at 1819.0 and 1814.7 cm^{-1} and a weaker band at 1795.2 cm^{-1}, labeled 5 (Figure 8). Pyrex photolysis produced new absorptions at 1870.7 and 1862.1 cm^{-1}, labeled 2, and a weaker absorption at 1784.6 cm^{-1}, labeled 4, and the absorption due to 5 increased 5-fold. Full arc photolysis allowed for further growth of 2 and 4 and a slight increase in 3, while 5 decreased slightly. Annealing caused the 5 absorption to disappear, one site absorption due to 3 decreased, one due to 2 increased, and the band labeled 4 decreased.

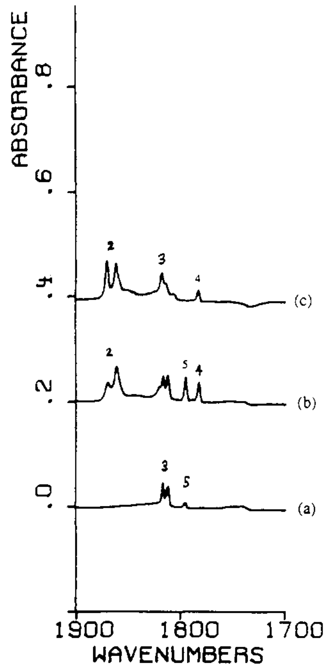

Figure 8. Infrared spectra in the 1900–1700-cm^{-1} region for sample in Figure 7.

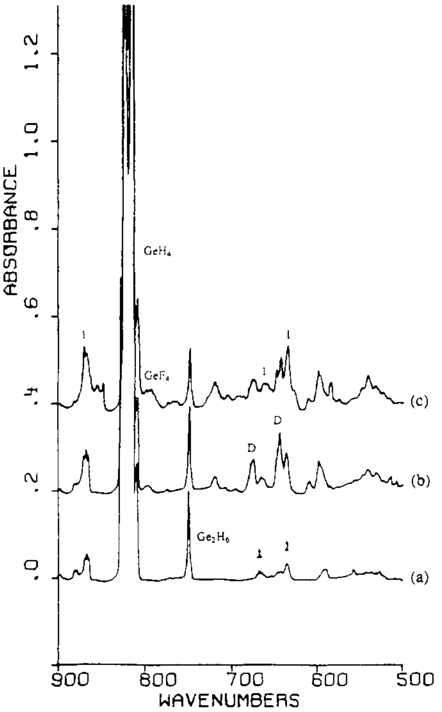

Figure 9. Infrared spectra in the 900–500-cm^{-1} region for sample in Figure 7.

The region from 900 to 500 cm^{-1} (Figure 9) revealed much photochemistry. Codeposition produced new absorptions at 880, 871.9, 867.4, 667.7, and 638.1 cm^{-1}, all labeled 1. In addition, an absorption[1] due to Ge_2H_6 was present at 751.2 cm^{-1}. Pyrex photolysis produced a slight growth in all the absorptions due to 1. A weak, broad band was produced at 531.0 cm^{-1}, and GeF_2, labeled D, was observed with splittings due to Ge isotopes in natural abundance at 679.1, 677.0, 675.3, 649.4, 647.4, and 645.2 cm^{-1}.[9] Furthermore, unidentified bands were produced at 721 and 598 cm^{-1}. Each band previously mentioned increased on full

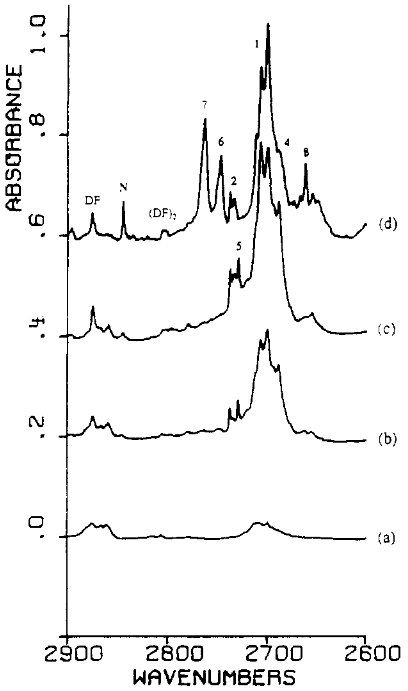

Figure 10. Infrared spectra in the 2900–2600-cm^{-1} region for Ar/GeD$_4$ = 200/1 and Ar/F$_2$ = 100/1 samples: (a) codeposited at 13 ± 1 K, (b) after 290–1000-nm photolysis, (c) after 220–1000-nm photolysis, and (d) after annealing to 30 ± 2 K.

arc photolysis with the exception of the impurity band. The bands labeled 1 showed only a 10–20% growth while the band labeled 4 showed nearly a 40% growth, GeF$_2$ absorptions more than doubled, and a weak GeF$_4$ band[9] was observed at 796 cm^{-1}. Annealing promoted slight growth of the bands labeled 1, caused little change in species 4, and decreased the GeF$_2$ absorptions. The GeF$_4$ absorption increased and new, unidentified absorptions were revealed at 855.2, 848.4, and 583.1 cm^{-1}.

GeD$_4$ + F$_2$. Two codeposition experiments were performed using GeD$_4$ and F$_2$. Infrared spectra are illustrated in Figures 10 and 11, and product absorptions are listed in Tables I–III. Absorptions labeled DF at 2896.1 and 2876.6 cm^{-1} are due to deuterium fluoride.[19] The broad band centered around 2804 cm^{-1}, labeled (DF)$_2$, is assigned to the dimer of deuterium fluoride, and the band labeled N at 2845.8 cm^{-1} belongs to the N$_2$--DF complex.[19]

In contrast to SiD$_4$, GeD$_4$ reacts with F$_2$ on codeposition, and mixed H/D experiments show that germanium hydride bonds are slightly more reactive (~15%) than germanium deuteride bonds based on the intensities of species 1 and the D counterpart of species 1. Codeposition (Figure 10a) produced a weak broad band centered at 2705 cm^{-1}. Pyrex photolysis (Figure 10b) produced a 10-fold increase and sharper bands at 2709.8 and 2703.1 cm^{-1}, labeled 1. Also, a strong shoulder at 2693.2 cm^{-1}, labeled 4, was revealed. Weaker absorptions were found at 2739.1 and 2732.1 cm^{-1}, labeled 2, and 5, respectively. Full arc photolysis (Figure 10c) allowed for further growth of bands belonging to species 1, 2, 4, and 5. Annealing (Figure 10d) produced sharp, new bands at 2764.7, 2748.9, and 2664.1 cm^{-1}, labeled 7, 6, and 8, respectively. The absorption due to 5 disappeared, the band labeled 4 decreased by over 50%, species 2 showed a slight decrease, and the absorptions due to 1 showed a slight growth.

The GeD stretching (Figure 11) region produced weak bands at 1312.5 and 1308.9 cm^{-1} on codeposition (labeled 3). Pyrex photolysis increased the yield of species 3 while also producing new absorptions at 1346.8, 1339.8, 1296.2, and 1287.8 cm^{-1}, labeled 2, 5, and 4, respectively. The band at 1274.4 cm^{-1} is due to CF$_4$ impurity in the F$_2$ sample.

The ν_5 region of GeD$_4$ (Figure 11) contained impurities due to different GeH$_x$D$_y$ molecules at 674.7 and 618.4 cm^{-1} and a band belonging to Ge$_2$D$_6$ at 542.4 cm^{-1}. Codeposition yielded new product absorptions at 668.0, 663.2, and 471.3 cm^{-1}, all attributed to 1. Pyrex photolysis increased the yield of 1 as well as producing new absorptions at 559.9 and 532.4 cm^{-1}. The GeF$_2$ absorptions, labeled D, became apparent at 679 and 645 cm^{-1}. Full arc photolysis produced an increased yield in all the product absorptions. Annealing succeeded in decreasing absorptions due to GeF$_2$ and 4 while those due to 1 showed little change.

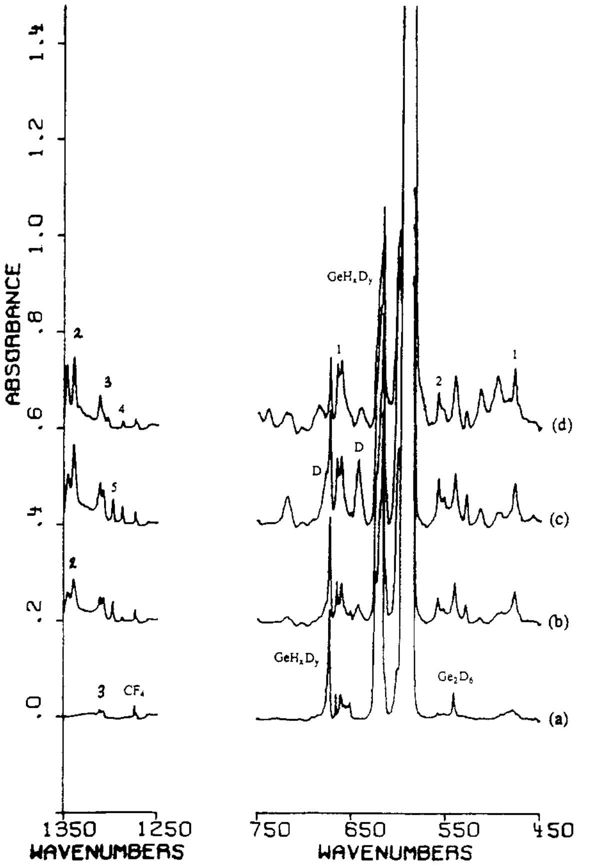

Figure 11. Infrared spectra in the 1350–1250- and 750–450-cm^{-1} regions for sample shown in Figure 10.

TABLE IV: Energies (hartrees) of Submolecules and Complexes Obtained from HONDO 7.0 ab Initio Calculations Using STO-3G and DZP Basis Sets

atom or molecule	STO-3G	DZP
F	-97.9865	-99.3977
HF	-98.5728	-100.0478
SiH$_2$	-286.6669	-290.0041
SiH$_3$	-287.2779	-290.6120
SiH$_4$	-287.9173	-291.2322
SiHF	-384.1711	-388.9668
SiH$_3$F	-385.3914	-390.1849
HSiH--HF	-385.2411	-390.0545
H$_2$Si--HF	-385.2454	-390.0581
H$_2$Si--FH	-385.2701	-390.0596
H$_3$Si--FH	-385.8517	-390.6599
H$_3$Si--HF	-385.9039	-390.6605
SiH$_3$--HF	-385.8514	-390.6610
SiH$_4$--HF	-386.4904	-391.2812
FSiH--FH	-482.7435	-489.0142
FSiH--HF	-482.7453	-489.0172
HFSi--HF	-482.7481	-489.0190
HSiF--HF	-482.7547	-489.0224
cyclic SiHF--HF	-482.7747	-489.0229
SiFH$_3$--FH	-483.9643	-490.2328
SiFH$_3$--HF	-483.9641	-490.2331
SiH$_3$F--HF	-483.9739	-490.2405

Calculations. Ab initio SCF-HF calculations using the HONDO 7.0 program[24,25] were performed on HF, SiH$_2$, SiH$_3$, SiH$_4$, SiH$_3$F, and several complexes between HF and these silicon species. Initially, STO-3G basis set calculations were run to obtain optimized geometries, and the energies are geometries were recalculated using double-ζ with polarization (DZP) basis sets (Tables

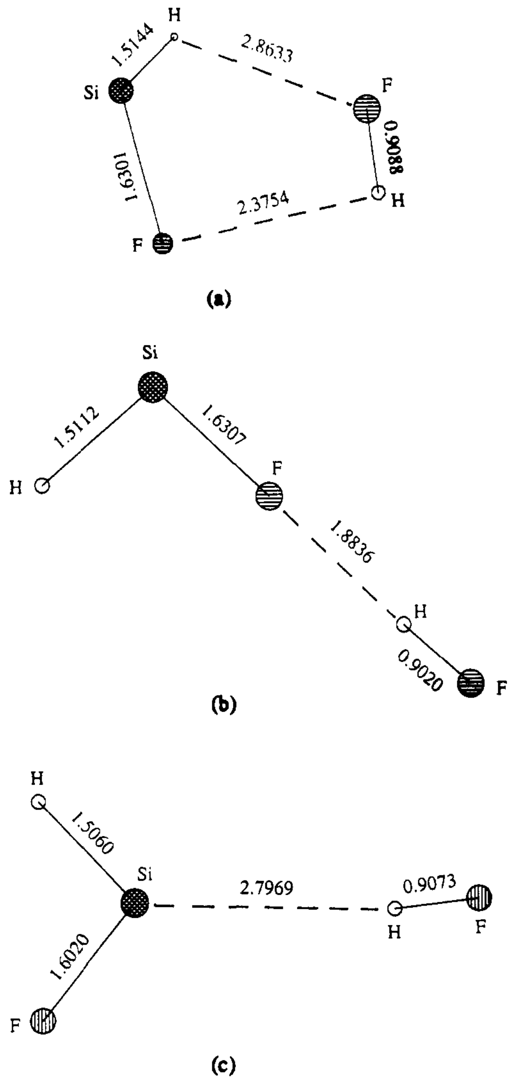

Figure 12. Structures of three HSiF--HF complexes with DZP calculated distances.

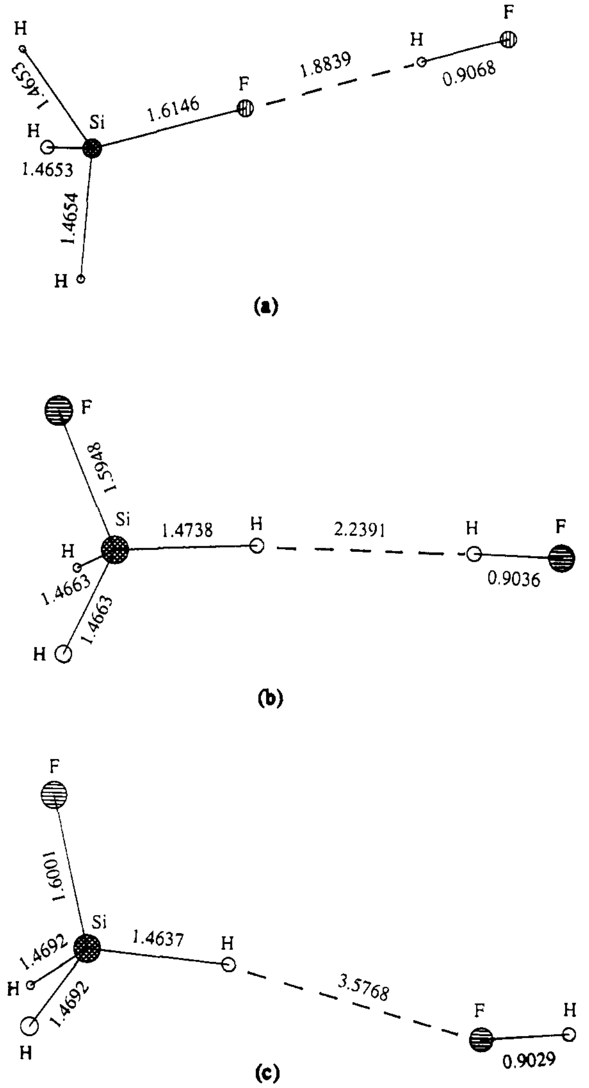

Figure 13. Structures of three SiH_3F--HF complexes with DZP calculated distances.

IV and V). Force constant calculations were carried out using the DZP optimized geometries to ensure that the structures and energies obtained were minima. Scaled HF fundamentals for the complexes are given in Table V; the scale factor used for HF frequencies was based on the observed matrix and DZP calculated values of HF, namely, 3919/4535 = 0.864. At this level of theory agreement with experiment cannot be more than qualitative. Since the present objective is not to get the most accurate structural parameters and energies but to aid in interpretation of experimental data, the DZP level of theory should predict the trends expected from more sophisticated calculations.

When combining HF with SiH_2, three isomers were considered, H_2Si--FH, H_2Si--HF, and HSiH--HF; in H_2Si--FH, the FH fragment is perpendicular to the H_2Si plane. Frequency calculations revealed scaled SiH stretching fundamentals at 1943, 2000, and 1967 cm^{-1} for H_2Si--FH, H_2Si--HF, and HSiH--HF, respectively. The HSiH--HF complex is 1.6 kcal/mol more stable than its individual components, but the stability gained in forming H_2Si--HF is 3.9 kcal/mol and that from H_2Si--FH is 4.8 kcal/mol.

Calculations for three isomers containing HF and SiH_3 were performed. Complexing the HF and SiH_3 submolecules leads to products which are 30, 420, and 700 cal/mol more stable for H_3Si--FH, H_3Si--HF, and SiH_3--HF, respectively. Owing to error in the calculated energies, these differences are not meaningful.

Calculations were done for five isomers containing HF and HSiF. The most stable isomer was a cyclic structure of HSiF--HF (Figure 12a). Initially, this calculation was started with HF perpendicular to the HSiF plane, but it collapsed to a planar ring structure in both STO-3G and DZP calculations. The cyclic structure is 340 cal/mol more stable than the open HSiF--HF complex (Figure 12b). The third most stable isomer of the series of HFSi--HF (Figure 12c), which is nearly 2.5 kcal/mol less stable than the cyclic form. The structures FSiH--HF and FSiH--HF are even less stable by 3.6 and 5.5 kcal/mol, respectively. The HSiF and HF submolecules yielded a cyclic complex structure which was 5.2 kcal/mol more stable than the combined energies of the individual components.

The last calculations were performed for HF and SiH_3F. The SiH_3F--HF arrangement (Figure 13a) proved to be much more stable than $FSiH_3$--HF (Figure 13b) and $FSiH_3$--FH (Figure 13c). The most stable product is 4.9 kcal/mol more stable than the combined energies of the individual components; the other two isomers are only 220 and 50 cal/mol more stable than the individual components, which are insignificant at this level of theory.

Discussion

Products of the fluorine and silane, and fluorine and germane codeposition reactions will be identified and reaction mechanisms discussed.

SiH_3F--HF. Codeposition of silane with fluorine yielded several new product bands, labeled 1, which increased on photolysis and further increased upon annealing. These new bands are assigned to SiH_3F--HF based on the infrared spectrum of SiH_3F, on H/D ratios of the observed bands, and on ab initio calculations. Gas-phase infrared spectra of silyl fluoride were obtained first by Newman et al. and later by Robiette et al. with deuteriated material.[26,27] Using the values from Robiette et al., ν_1 occurs at 2206 cm^{-1}, ν_2 at 991 cm^{-1}, ν_3 at 875 cm^{-1}, ν_4 at 2209 cm^{-1}, ν_5

TABLE V: Bond Distances (Å) and Angles (deg) of Submolecules and Complexes and Corrected HF Fundamentals (cm^{-1}) Obtained from HONDO 7.0 ab Initio Calculations Using the DZP Basis Set

molecule	r(HF)	r(SiH)	r(SiF)	complex bond	∠HSiH or ∠HSiF	scaled ν_s(HF)[a]
HF	0.903					3919
SiH_2		1.510			93.4	
SiH_3		1.476			110.9	
SiH_4		1.476			109.5	
SiHF		1.516	1.610		96.8	
SiH_3F		1.468	1.598		110.6	
HSiH--HF	0.905	1.508 1.519		2.062	92.8	3859
H_2Si--HF	0.909	1.501		2.719	95.6	3772
H_2Si--FH	0.907	1.512		2.450	93.4	3849
H_3Si--FH	0.903	1.476		4.043	110.7	3899
H_3Si--HF	0.904	1.472 1.472		3.207	111.9	3876
SiH_3--HF	0.904	1.473 1.479		2.215	110.2	3882
SiH_4--HF	0.904	1.473 1.480		2.327	109.0	3883
FSiF--FH	0.903	1.512	1.611	3.346	97.1	3900
FSiH--HF	0.905	1.528	1.605	2.001	96.2	3852
HFSi--HF	0.907	1.506	1.602	2.797	98.1	3806
HSiF--HF	0.902	1.511	1.631	1.884	96.0	3831
cyclic HSiF--HF	0.909	1.514	1.630	1.630	96.3	3818
$SiFH_3$--FH	0.903	1.469 1.464	1.600	3.577	111.0	3900
$SiFH_3$--HF	0.904	1.466 1.474	1.595	2.239	109.8	3887
SiH_3F--HF	0.907	1.465 1.465	1.615	1.884	111.4	3835

[a] Calculated frequencies were scaled using a factor of 3919/4535 or 0.8642.

at 961 cm^{-1}, and ν_6 at 729 cm^{-1}. The values for the product absorptions differ since the sample is contained in solid argon, and also since the product is complexed with HF. To rationalize the interaction with HF, previous work and ab initio calculations were considered. Work with fluorine and methane by Johnson and Andrews[16] suggested that the most stable bonding of HF with CH_3F is through a hydrogen bond to the fluorine atom of CH_3F, i.e., CH_3F--HF. In addition, ab initio calculations showed SiH_3F--HF to be more stable than other arrangements by more than 4.5 kcal/mol (see Table I). Considering bonding in this complex, Si–H stretching motions are expected to blue shift while the Si–F stretch is expected to red shift. The Si–H stretching modes blue shift from 2206 and 2209 cm^{-1} for ν_1 and ν_4, respectively, of gas-phase SiH_3F to 2241 and 2257 cm^{-1}, respectively, for SiH_3F--HF. The ν_3(Si–F) stretching mode red shifts over 81 cm^{-1} from the gas-phase value to 793 cm^{-1}.

Unlike the fluorine and methane work where photolysis was required to give product absorptions, silane reacted with F_2 on codeposition. The values listed in columns 1 and 2 of Table I are absorptions whose band intensities increased at similar rates upon photolysis and annealing. The HF stretch associated with the complex was easy to discern since it was the most intense product absorption in the spectrum and since it too formed upon codeposition and increased with photolysis and annealing. Furthermore, the location of the HF stretching frequency ν_s shows excellent agreement with ab initio calculations, and the HF librational motion, ν_l, is appropriate for HF in this hydrogen bonding environment.[28]

Further evidence for the assignment was obtained by comparing H/D ratios of the complex with the gas-phase H/D ratios of silyl fluoride. The H/D ratios for ν_1 to ν_6 fundamentals, respectively, of gas-phase SiH_3F are 1.3980, 1.3958, 0.9843, 1.3678, 1.3689, and 1.3230 while SiH_3F--HF shows H/D ratios of 1.3657, 1.3871, 0.9950, 1.3702, 1.3768, and 1.3369 for ν_1 to ν_6, respectively. In addition, the HF stretch shows an H/D shift of 1.3630 versus a 1.3625 ratio for isolated HF and DF.[19] Experimental and calculated band intensities of the various modes of SiH_3F were also helpful in determining product absorptions of the complex.

GeH_3F--HF. The germyl fluoride complex with HF was expected to show similar behavior as the SiH_3F--HF complex. The infrared spectrum of GeH_3F provides a starting point for the GeH_3F submolecule[29] in the GeH_3F--HF complexes. The spectrum of GeD_3F was also helpful in making assignments to the GeD_3F--DF complex. Displacements for the GeH_3F and GeD_3F submolecules in the complexes followed their silicon analogs.

Germane reacted with fluorine on codeposition. Like SiH_3F--HF, GeH_3F--HF formed upon codeposition and grew further with photolysis and annealing. The bands in columns 3 and 4 of Table I showed similar growth patterns. For example, the ν_1 and ν_4 modes of SiH_3F--HF were found to be blue of the ν_3 mode of isolated SiH_4. In addition, the ν_4 mode of SiH_3F--HF was more intense than the ν_1 mode of the same complex due to antisymmetric nature of the mode. In considering GeH_3F--HF, the ν_1 and ν_4 modes were expected to be found above the ν_3 mode of GeH_4. As it turned out, the ν_1 and ν_4 modes of GeH_3F--HF were not intense enough to be observed, but these modes were observed for GeD_3F--DF.

SiH_2 Complexes. Assignments to SiH_2 complexes are more difficult. Early work by Milligan and Jacox[2] assigned SiH stretching motions of SiH_3 below SiH stretching motions of SiH_2; however, Fredin et al.[11] offered completely different assignments for SiH_2 absorptions. After analyzing the spectra from these works and considering ab initio calculations, the later assignments by Fredin et al. are believed to be correct. Ab initio calculations performed here show that SiH stretching frequencies decrease for the series SiH_4, SiH_3, SiH_2, SiH. This is in agreement with calculations performed by Sahu et al. as well.[30] Furthermore, ab initio calculations also suggest that Si–H stretching modes of SiH_3 are very close to that of SiH_4 and that the modes are very weak. So, there is a good chance that the ν_1 and ν_3 modes of SiH_3 will be masked by SiH_4 absorption in these experiments.

Given this, the ν_1 and ν_3 modes of SiH_2 occur at 1964.4 and 1973.3 cm^{-1}, respectively.[11] The product absorptions at 1985.7 and 1942.8 cm^{-1} are most likely due to SiH_2 complexes with HF or $(HF)_2$. The SiH_2 complexes with HF bonded to silicon were calculated to be of comparable stability; however, the associated 3828.6-cm^{-1} ν_s(HF) mode is *too low* for the hydrogen in HF to be free. The H_2Si--HF and/or H_2Si--$(HF)_2$ complexes are likely for species 2 and 3, but their structures cannot be determined. In addition H/D ratios are reasonable for the ν_s and ν_3 modes of the complexes. Experimental data shows an H/D ratio of 1.3712 for the ν_3 mode of SiH_2. The H/D ratios for the ν_3 modes are 1.3711 and 1.3637 for complexes 2 and 3, respectively. The H/D ratios for the ν_s mode is 1.3680 as compared to the 1.3625 ratio for isolated HF and DF.

GeH_2 Complexes. Identification of GeH_2 complexes with HF and $(HF)_2$ in Table II were made using similar rationale as for the SiH_2 complexes. As for SiH_2 and SiH_3, assignments for GeH_2 and GeH_3 appear to be incorrect. Smith and Guillory[3] misassigned bands because of correlating with the work of Milligan and Jacox,[2] whose assignments, as discussed previously, are incorrect. From the observation of Smith and Guillory, bands at 1839 and 1813 cm^{-1} are probably due to ν_3 and ν_1 of GeH_2, respectively. If this conclusion is correct and the assignments of SiH_2 with HF are correct, then the same arguments used for the SiH_2 complexes can be used for the GeH_2 complexes. The bands labeled 2 and 3 are probably due to GeH_2 complexes with HF or $(HF)_2$, but we cannot determine the structures.

HSiF Complexes. Ismail et al. measured ν_1, ν_2, and ν_3 of HSiF at 1913.1, 859.0, and 833.7 cm^{-1}, respectively, while DSiF modes shifted to 1387.4, 638.3, and 833.4 cm^{-1}, respectively.[31] In the SiH stretching region, a product band was observed at 1908.0 cm^{-1}. This might belong either to SiH_2 or SiHF complexes with HF, but bands at 865.5 and 751.6 cm^{-1} seemed to change along with the 1908.0-cm^{-1} band. The location of two bands outside of the SiH stretching region strongly indicates that these absorptions are due to HSiF complexes with HF. The H/D ratios for ν_1 and ν_s of the complex are 1.3772 and 1.3632, respectively. The H/D ratio for the same modes of isolated HSiF and HF are 1.3789 and 1.3625, respectively.

Ab initio calculations suggest that the most stable arrangements of HSiF with HF are cyclic or open HSiF--HF (see Figure 13). Frequency calculations of the cyclic isomer predict slight blue shifts in the ν_1 and ν_2 modes and a large red shift for the SiF stretching mode. The absorptions, labeled 4, are tentatively assigned to cyclic HSiF--HF since it is the most stable arrangement based on ab initio calculations.

HGeF Complexes. One variation in the chemistry of SiH_4 and GeH_4 was an additional band in the GeH stretching region at 1795.2 cm^{-1} near isolated HGeF. The 1795.2-cm^{-1} band disappears completely on annealing and most certainly is not associated with the 1784.6-cm^{-1} band in the GeH stretching region of HGeF. There appear to be two HGeF complexes produced in these experiments. Comparison of the GeH stretching region to the SiH stretching region suggests the band at 1784.6 cm^{-1} for the cyclic isomer HGeF--HF. The band at 1795.2 cm^{-1}, labeled 5, is tentatively assigned to HGeF--HF simply because calculations give another isomeric form, HSiF--HF, to be only slightly less stable than the cyclic form. Assuming that Ge containing complexes behave in a similar manner as Si containing complexes, HGeF--HF too would be nearly as stable as cyclic HGeF--HF. The similarity of band behavior leads to tentative assignment of the band at 3717.2 cm^{-1} to the ν_s mode of HGeF--HF.

SiH_3 Complexes. Evidence for SiH_3 complexes is minimal. Calculations suggest that the SiH stretching modes of SiH_3 containing complexes are buried under the ν_3 mode of SiH_4. However, experiments by Jacox[15] and by Johnson and Andrews[16] with CH_4 and F produced CH_3--HF on diffusion and reaction of F atoms with CH_4. There is an equally good a chance that SiH_3 or GeH_3 bonded to HF will be a product in these experiments. The band at 3846 cm^{-1}, labeled 6, that appeared on annealing, is tentatively assigned to $(SiH_3)(HF)$. Unfortunately, deuteriated silane experiments failed to produce a comparable absorption indicating that the cold F atom reaction with SiD_4 is less favorable than with SiH_4.

GeH_3 Complexes. Using similar arguments presented for the SiH_3 case, the product bands at 3745 and 3772 cm^{-1}, labeled 6 and 7, are tentatively assigned to $(GeH_3)(HF)$ complexes. The deuterium counterparts were observed at 2749 and 2765 cm^{-1} for the F and GeD_4 reaction.

Other Species. A strong absorption was observed at 836.8 cm^{-1}, which showed no shift from H to D experiments. Since the gas-phase SiF fundamental[32] is 847.7 cm^{-1}, the 836.8-cm^{-1} band is probably due to SiF in solid argon. The observation of SiF, SiF_2, SiF_3, and SiF_4 attests to the great reactivity of SiH_4 and F_2. The bands labeled 8 in SiH_4 and GeH_4 experiments appeared on annealing and are likely due to higher order 1/2 complexes such as SiH_3F--$(HF)_2$ and GeH_3F--$(HF)_2$. Note the displacement to lower frequency from the analogous 1/1 complexes as has been discussed for a number of HF complexes.[28]

Reactions. The first evidence of product formation came upon codeposition of SiH_4 and F_2, which gave the SiH_3F--HF product, 1. The Si–H and F–F bonds are weak enough for the formation of Si–F and H–F to drive the reaction. This reaction does not occur as readily with SiD_4. In this case photolysis of F_2 was required to drive the reaction to form SiD_3F--DF:

$$(SiH_4)(F_2) \xrightarrow{\text{reaction and photolysis}} (SiH_3F\text{--}HF)^* \rightarrow SiH_3F\text{--}HF$$

$$\rightarrow SiH_2\text{--}HF + HF \text{ and/or } SiH_2\text{--}(HF)_2$$

$$\rightarrow HSiF\text{-}HF + H_2$$

$$? \rightarrow H_2SiF\text{--}HF + H$$

$$SiH_4 + F \xrightarrow{\text{annealing}} (SiH_3)(HF)$$

The $(SiH_3F$--$HF)^*$ species is formed with excess internal energy owing to the strong Si–F bond. Although the matrix is expected to quench rapidly this internal energy as attested by the strong product 1 bands, hydrogen atom elimination from silicon could also occur to give the radical complex SiH_2F--HF. Although no conclusive evidence was found for this species, the spectra are complicated and such a species could be produced. There is, however, evidence for the HSiF--HF complex in the spectra, and this species most likely arises from H_2 elimination from silicon in the primary photochemical reaction of $(SiH_4)(F_2)$.

Codeposition also allows for the formation of divalent silicon hydride complexes H_2Si--HF and/or H_2Si--$(HF)_2$, if the second F atom abstracts hydrogen rather than adds to silicon. Here, two SiH bonds are broken, but two HF molecules are formed, and if an HF molecule does not escape the cage, a hydrogen bond between the two HF fragments is also formed. Again, the driving force is the formation of the extremely stable HF product. Complexes (HSiF)(HF) and the germane counterparts are also produced upon photolysis.

Finally, complexes were formed on annealing which allows trapped F atoms to diffuse and react. These products are believed to be trivalent silicon hydride complexes $(SiH_3)(HF)$. As evidenced by the marked growth of FO_2 at 1489 cm^{-1}, annealing favors single F atom reactions. One F atom abstracts a hydrogen to form HF, which then bonds to the SiH_3 fragment in an energetically favorable way.

Conclusion

Matrix experiments were performed to study reactions of F_2 with SiH_4 and GeH_4. Codeposition allowed for the formation of SiH_3F--HF and divalent silicon hydride complexes H_2Si--HF or H_2Si--$(HF)_2$ and HSiF--HF, as the formation of HF provided the driving force for the reaction. Photolysis into the ultraviolet absorption of fluorine markedly increased these product absorptions. Annealing allowed the fluorine atom reaction product $(SiH_3)(HF)$ to be formed.

Some interesting chemistry was displayed by these systems. First, hydrides were found to be more reactive than deuterides as expected. Comparison of Figure 1a and Figure 7a shows comparable yields of species 1 in SiH_4 and GeH_4 experiments. It might be expected that hydrogen abstraction from GeH_4 would be more facile since the Ge–H bond is weaker than the Si–H bond,[33] and O atom reactions with GeH_4 are 3–4 times faster than with SiH_4,[34] although F atom reactions with GeH_4 and SiH_4 have the same rate constant within experimental error.[35]

Another interesting observation is that the HF stretches for complexes containing Ge are 100–130 cm^{-1} lower than their Si counterparts; this lower HF stretching mode implies a greater interaction with the Ge containing submolecule. For example, in GeH_3F--HF, the HF stretching mode occurs at 3677 cm^{-1}, whereas in SiH_3F--HF, the ν_s mode occurs at 3809 cm^{-1}; therefore GeH_3F is a stronger base than SiH_3F. In other words, there is more electron density on the F atom of the GeH_3F submolecule to provide for a stronger interaction with HF. This follows from the increase in electropositive nature of Ge as compared to Si. Germane itself interacts slightly more strongly with HF than silane in this regard.[6] Finally, SiF was produced whereas GeF was not, and the yield of SiF_4 was substantially greater than the yield of GeF_4. This can be accounted for by the fact that an SiF bond is energetically stronger and a higher degree of fluorination was observed for SiH_4 than for GeH_4 in these experiments.

Acknowledgment. We gratefully acknowledge financial support from N.S.F. Grant CHE 88-20764.

References and Notes

(1) Wilde, R. E.; Srinivasan, T. K. K.; Harral, R. W.; Sanker, S. G. *J. Chem. Phys.* **1971**, *55*, 5681.
(2) Milligan, D. E.; Jacox, M. E. *J. Chem. Phys.* **1970**, *52*, 2594.
(3) Smith, G. R.; Guillory, W. A. *J. Chem. Phys.* **1972**, *56*, 1423.
(4) Withnall, R.; Andrews, L. *J. Phys. Chem.* **1985**, *89*, 3261.
(5) Withnall, R.; Andrews, L. *J. Phys. Chem.* **1990**, *94*, 2351.
(6) Davis, S. R.; Andrews, L. *J. Chem. Phys.* **1987**, *86*, 3765.
(7) Milligan, D. E.; Jacox, M. E. *J. Chem. Phys.* **1968**, *49*, 4269.
(8) Milligan, D. E.; Jacox, M. E.; Guillory, W. A. *J. Chem. Phys.* **1968**, *49*, 5330.
(9) Hastie, J. W.; Hauge, R.; Margrave, J. L. *J. Phys. Chem.* **1968**, *72*, 4492.
(10) Huber, H.; Kundig, E. P.; Ozin, G. A.; Vander Voet, A. *Can. J. Chem.* **1974**, *55*, 95.
(11) Fredin, L.; Hauge, R. M.; Kafafi, Z. H.; Margrave, J. L. *J. Chem. Phys.* **1985**, *82*, 3542.
(12) Yamada, C.; Hirota, E. *Phys. Rev. Lett.* **1986**, *56*, 923.
(13) Yamada, C.; Kanamori, H.; Hirota, E.; Nishiwaki, N.; Itabashi, N.; Kato, K.; Goto, T. *J. Chem. Phys.* **1989**, *91*, 4582.
(14) Hudgens, J. W. *J. Chem. Phys.* **1991**, *94*, 5331.
(15) Jacox, M. E. *Chem. Phys.* **1979**, *42*, 133.
(16) Johnson, G. L.; Andrews, L. *J. Am. Chem. Soc.* **1980**, *102*, 5736.
(17) Andrews, L.; Johnson, G. L. *J. Chem. Phys.* **1982**, *76*, 2875.
(18) Johnson, G. L.; Andrews, L. *J. Am. Chem. Soc.* **1982**, *104*, 3043.
(19) Andrews, L.; Johnson, G. L. *J. Phys. Chem.* **1984**, *88*, 425.
(20) Ayers, G. P.; Pullin, A. D. E. *Spectrochim. Acta, Part A* **1976**, *32*, 16220.
(21) Redington, R. L.; Milligan, D. E. *J. Chem. Phys.* **1962**, *37*, 2162.
(22) Jones, L. H.; Swanson, B. I.; Ekberg, S. A. *J. Chem. Phys.* **1984**, *81*, 5268.
(23) Arkell, A. *J. Am. Chem. Soc.* **1965**, *87*, 4057.
(24) Dupuis, M.; Watts, J. D.; Villar, H. O.; Hurst, G. J. B. *Comput. Phys. Commun.* **1989**, *52*, 415.
(25) Dupuis, M.; Phys, J.; King, H. F. *J. Chem. Phys.* **1976**, *65*, 111.
(26) Newman, C.; O'Loane, J. K.; Polo, S. R.; Wilson, M. K. *J. Chem. Phys.* **1956**, *25*, 855.
(27) Robiette, A. G.; Cartwright, G. J.; Hoy, A. R.; Mills, I. M. *Mol. Phys.* **1971**, *20*, 541.
(28) Andrews, L. *J. Phys. Chem.* **1984**, *88*, 2940.
(29) Freeman, D. E.; Rhee, K. H.; Wilson, M. K. *J. Chem. Phys.* **1963**, *39*, 2908.
(30) Sahu, S. N.; Shi, T. S.; Ge, P. W.; Corbett, J. W.; Hiraki, A.; Imura, T.; Tashiro, M.; Singh, V. A. *J. Chem. Phys.* **1982**, *77*, 4330.
(31) Ismail, Z. K.; Fredin, L.; Hauge, R. H.; Margrave, J. L. *J. Chem. Phys.* **1982**, *77*, 1626.
(32) Huber, K. P.; Herzberg, G. *Constants of Diatomic Molecules*; Van Nostrand Reinhold: New York, 1979.
(33) Cotton, F. A.; Wilkinson, G. *Advanced Inorganic Chemistry*, 4th ed.; John Wiley and Sons: New York, 1980.
(34) Agrawalla, B. S.; Setser, D. W. *J. Chem. Phys.* **1987**, *86*, 5421.
(35) Agrawalla, B. S.; Setser, D. W. *Gas Phase Chemiluminescence and Chemiionization*; Fontijn, A., Ed.; Elsevier Science Publishers: Amsterdam, 1985.

Infrared Spectra and Structure of Acetylene on NaCl(100)

S. Keith Dunn and George E. Ewing*

Department of Chemistry, Indiana University, Bloomington, Indiana 47405 (Received: November 26, 1991; In Final Form: March 10, 1992)

Infrared spectra of C_2H_2 and C_2D_2 on NaCl(100) are reported. Isotherms are presented for 78, 84, and 95 K. The isosteric heat of adsorption for $\Theta = 0.5$ is -30 ± 2 kJ/mol, while the interaction energy between adsorbates is -4 kJ/mol. The ν_3 band of acetylene is split into three peaks. Multiple peaks for this nondegenerate vibration result from both correlation-field and static-field splittings. The spectra are qualitatively explained by a bilayer structure similar to 1.5 layers of the low-temperature crystalline phase of acetylene.

Introduction

Infrared spectroscopy is useful for determining the structure of molecules adsorbed onto alkali halide surfaces.[1-6] While diffraction methods provide information about the adlayer lattice sites, they tell little about molecular orientations. Polarized IR studies are needed to supply this information. From these IR studies, structures have been proposed for CO[3,5] and CO_2[4,6] on NaCl(100).

At submonolayer coverages in the high-temperature phase, CO molecules are randomly distributed among all available adsorption sites of NaCl(100) because the adsorbates exhibit little interaction among neighbors. This ideal lattice gas gives rise to Langmuir isotherms.[7] However, the case of CO_2 on NaCl is qualitatively different. Because of interactions among the adsorbed molecules, CO_2 grows in constant-density islands, and the monolayer structure closely resembles one layer of the molecular crystal.[4,6] These interactions, which lead to non-Langmuir isotherms, are successfully modeled by a molecular quadrupole–quadrupole approximation.[6]

Acetylene, like CO_2, possesses a large permanent molecular quadrupole moment, but, unlike CO_2, exhibits hydrogen bonding in condensed phases.[8-22] The dominant surface–adsorbate force for acetylene on NaCl is expected to result from electric field gradient–quadrupole interactions. The adsorbate–adsorbate interactions are likely quadrupole–quadrupole and hydrogen bonding. Since the same types of forces govern the adsorbed phase, molecular crystals and van der Waals complexes, structural similarities are anticipated. In particular the characteristic T-shape between neighboring molecules in the condensed phases and clusters of acetylene is likely to occur.[8-13]

Schinzer reported spectra from acetylene adsorbed onto polycrystalline NaCl films. Since the ν_5 bending mode produced only one peak, he concluded that the degeneracy of this mode was not lifted upon adsorption, and therefore the molecular axis of acetylene is perpendicular to the substrate.[1] While the arguments used in this discussion were appropriate, the bandwidth discussed was approximately 20 cm^{-1} and could obscure splittings of spectroscopic features.

By use of a single-crystal apparatus which employs plane polarized light, it has recently become possible to obtain spectral features with full width at half maximum (fwhm) below 0.1 cm^{-1} for small molecules adsorbed onto NaCl(100).[2-6,23,24] In this paper

0022-3654/92/2096-5284$03.00/0 © 1992 American Chemical Society